

FATIGUE FRACTURE IN PLATES IN TENSION AND OUT-OF-PLANE SHEAR*

Alan T. Zehnder[†], Mark J. Viz[‡] and Yogesh Potdar
Department of Theoretical and Applied Mechanics
Cornell University, Ithaca, NY 14853
(607)255-9181, (607)255-2011 (fax), atz2@cornell.edu

January 6, 2000

Abstract

Straight cracks near a stiffening element, or curved cracks, in a pressurized shell can be subjected to out-of-plane tearing stresses in addition to normal tensile stresses due to the membrane stresses in the shell. To predict the rate of fatigue crack growth in such situations a theory and a crack growth rate correlation are needed. Such loadings are modeled as a superposition of plane stress tensile fracture, (Mode-I) and Kirchhoff plate theory shearing fracture (Mode-2). Finite element analyses using shell elements are used to compute the energy release rate and stress intensity factors associated with the loading. Three fatigue crack growth rate experiments were carried out on sheets of 2024-T3 aluminum alloy loaded in tension and torsion. The first set of experiments are constant amplitude fatigue crack growth tests. The second consists of experiments where crack closure is artificially eliminated to determine the rate of crack growth in the absence of crack face contact. The third is a set of constant stress intensity factor amplitude tests. The results all show that as the crack grows extensive crack face contact occurs, retarding crack growth. In the absence of crack face contact, however, the addition of out-of-plane shear loading increases the crack growth rate substantially.

Keywords - fatigue fracture; plate theory; aluminum 2024; finite element method, contact, friction, mixed-mode fracture

NOMENCLATURE

a	=	crack length
C	=	Paris law constant
E	=	Young's modulus
F_i	=	nodal forces
G_i	=	components of energy release rate corresponding to i th nodal degree of freedom
G_{K_I}	=	component of energy release rate corresponding to tensile loading
G_{k_2}	=	component of energy release rate corresponding to out – of – plane shear loading
h	=	plate thickness
k_1	=	Kirchhoff theory Mode – 1 stress intensity factor

*accepted in *Fatigue and Fracture of Engineering Materials and Structures*.

[†]corresponding author

[‡]currently at GATX, Chicago

k_2	=	Kirchhoff theory Mode – 2 stress intensity factor
K_I	=	plane – stress Mode – I stress intensity factor
K_{II}	=	plane – stress Mode – II stress intensity factor
m	=	Paris law exponent
N	=	number of cycles
P	=	axial load
r	=	distance to the crack tip
R	=	ratio of min to max load or stress intensity factor
T	=	torque
u_i	=	nodal displacements
x_i	=	Cartesian coordinates
w	=	out of plane displacement
ν	=	Poisson's ratio
σ_{ij}	=	ij components of stress
θ	=	polar coordinate angle

1 INTRODUCTION

This work stems directly from concerns regarding fracture along a lap joint in a pressurized aircraft fuselage. In this scenario, material near the tip of a through crack along the lap joint is loaded in a combination of in-plane tension from the hoop stresses in the fuselage skin and out-of-plane shear from the internal pressure "pushing out" on the skin. One side of the crack is much stiffer than the other side. The less stiff side bulges out, resulting in tearing stresses at the crack tip.

At the outset of the author's research little was known about fracture and fatigue in plates and shells under tension and out-of-plane shear. Thus, to answer the question of what is the fatigue crack growth rate at a lap joint, a program of research was begun in 1991 and carried out over the next five years to study the theory for describing such fractures and for correlating experimental data, to study the procedures for computing the relevant crack tip loading parameters, and to experimentally study fatigue crack growth under tension and out-of-plane shear loading. Prior results are contained in [1, 2, 3, 4, 5, 6, 7]. Extensive reviews of work prior to 1991 can be found in [1, 2].

The crack tip stresses are described as a superposition of the plane stress Mode-I and the plate theory out-of-plane shearing stresses. For a through crack in a thin plate, the out-of-plane shearing produces predominantly Mode-II like stresses instead of Mode-III like stresses. This applies to thin plates only. The stress intensity factors associated with this superposition are computed using the modified crack closure method in conjunction with geometrically nonlinear finite element analyses. Tension-torsion fatigue fracture experiments were performed on edge notched plates to simulate the loading of a cracked, pressurized lap joint. Results of these experiments show that there is considerable crack face contact. This contact tends to shield the crack tip from the full measure of stresses that would be present in the absence of contact. Thus the rate of fatigue crack growth can be greatly reduced compared to pure tensile loading. Experiments to determine the rate of growth in the absence of contact and to quantify the shielding were performed as well.

2 THEORY

Fatigue crack growth is determined by the cyclic stress and strain fields in the immediate vicinity of the crack tip. Thus in order to understand the behavior of cracked plates and to correlate experimental data, the crack tip fields must be understood. The crack tip fields are inherently three dimensional, and in principle

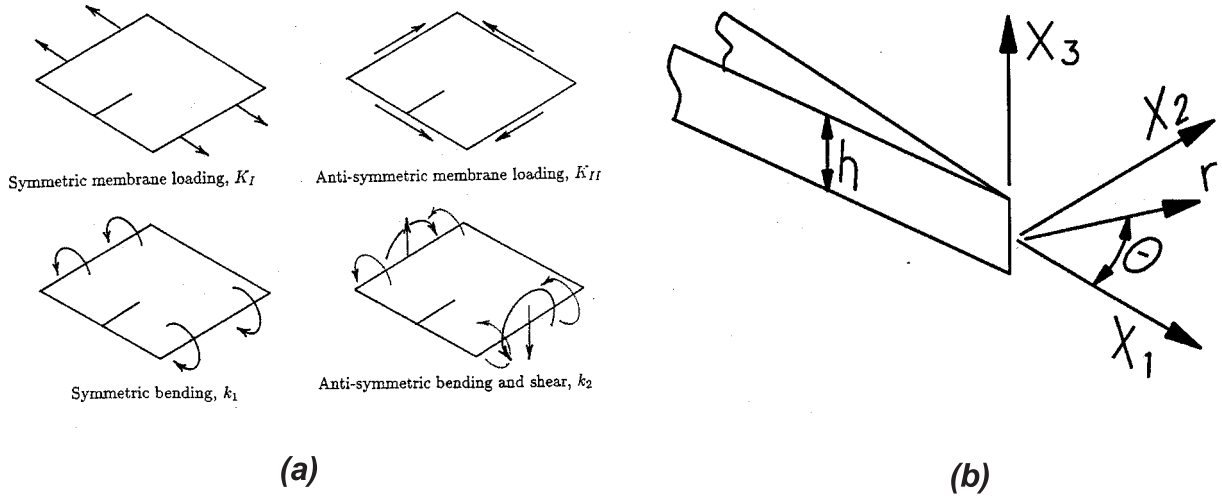


Figure 1: (a) Membrane, bending and transverse shear fracture modes for a plate with a straight through crack. Stress intensity factors corresponding to each mode are shown. (b) Crack tip coordinate system.

could be determined numerically for each particular situation using three dimensional numerical analyses. Such an approach, however is not only difficult from the engineering point of view, but gives little general insight into the nature of the crack tip fields. Instead, assuming linear elastic material behavior, analytical models of the crack tip stress state can be constructed using a large deflection plate theory that couples the in-plane or membrane stresses to the out-of-plane or bending stresses.

Such models can assume either Kirchhoff or Reissner plate theory kinematics. The Kirchhoff theory is simpler, but due to the kinematic assumption that lines perpendicular to the plate surface remain perpendicular (analogous to plane sections remain plane in beam theory), stress free boundary conditions on the crack cannot be exactly satisfied [8, 9]. By allowing lines perpendicular to the plate to rotate and deform, the Reissner theory [10, 11] introduces additional kinematic flexibility that allows stress free boundary conditions to be satisfied exactly. Thus it would appear that the Reissner theory is a better choice for describing the crack tip stress fields. However, it is known that solutions from the Reissner and Kirchhoff theories differ near free edges only in a boundary layer of extent on the order of the plate thickness. Within this boundary layer, for ductile materials, plastic deformation occurs, thus neither elastic plate theory is valid. Furthermore, in the limit as the plate thickness goes to zero the energy release rate is the same from either theory [12]. Thus in ref. [2] it is argued that consistent with the small scale yielding approach to fracture, the Kirchhoff theory is a better choice for correlating the fracture behavior in thin plates; it correctly describes the stress field in a region outside the crack tip plastic zone, provides the correct energy release rate, and is easily used for engineering analyses.

Using the large deflection von-Karman plate theory (which assumes Kirchhoff like kinematics) Hui and Zehnder [13] showed that the crack tip deformation fields can be described as a superposition of plane stress and Kirchhoff plate theory fields. As defined in Figure 1a, for general loadings of thin, cracked plates under membrane and out-of-plane loads, two fracture modes with corresponding stress intensity factors, K_I , and K_{II} can be identified with the crack tip membrane stresses, and two fracture modes, with stress intensity factors, k_1 , and k_2 can be identified with the crack tip bending stresses. Analyses show that the two important fracture modes for the lap joint problem are the membrane K_I , and the out-of-plane k_2 . Note that superficially the out-of-plane k_2 mode is similar to the anti-plane shear theory Mode-III. However, Mode-III is strictly valid only for plates of infinite thickness since at the free surfaces of the plate the traction must

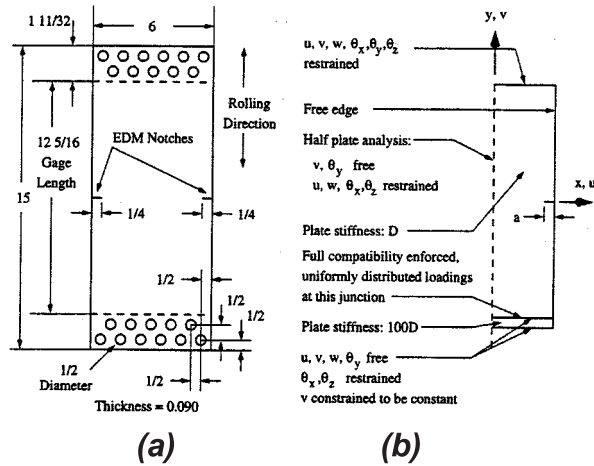


Figure 2: (a) Dimensions of the double edge notched tension-torsion test specimen, given in inches. (b) Boundary conditions used for half-plate finite element simulation of the test specimen.

be zero, which (except for trivial solutions) violates the assumptions of the anti-plane shear theory. Thus the out-of-plane k_2 mode is separate from, but in some ways related to Mode-III.

In mixed mode problems, the crack tip fields can be described as a superposition of stress intensity factors from linear theories. However, in a fuselage, and in our test specimen, the deflection of the plate will be large, and thus nonlinear analyses are required [13] to correctly compute the stress intensity factors. In this work geometrically nonlinear analyses are used. The results from the nonlinear analysis are then drawn into the local model that characterizes the crack tip stress field in terms of a superposition of stress intensity factors from the Kirchhoff and plane-stress theories.

Assuming that the crack tip stresses are a superposition of the stresses from the membrane and out-of-plane loads, the stresses on a plane ahead of the crack ($\theta = 0$ in Figure 2) are [9, 14, 15]

$$\begin{aligned}
 \sigma_{22} &= \frac{K_I}{\sqrt{2\pi r}} + \frac{k_1}{\sqrt{2r}} \frac{2x_3}{h}, \\
 \sigma_{21} &= \frac{K_{II}}{\sqrt{2\pi r}} + \frac{k_2}{\sqrt{2r}} \left(\frac{1+\nu}{3+\nu} \right) \frac{2x_3}{h}, \\
 \sigma_{23} &= \frac{-k_2 h}{2(2r)^{3/2}(3+\nu)} \left[1 - \left(\frac{2x_3}{h} \right)^2 \right],
 \end{aligned} \tag{1}$$

where ν is the Poisson ratio, h is the plate thickness, and the stress intensity factors, K_I , K_{II} , k_1 , and k_2 are defined in Figure 1. Note that the in plane stresses have a contribution from both the membrane and plate theory stress intensity factors. The out-of-plane shear stress is determined by the plate theory Mode-2 (k_2) stress intensity factors, and has an $r^{-3/2}$ singularity, due to the assumptions of the Kirchhoff plate theory. Fatigue crack growth is assumed to depend exclusively on the cyclic values of the above stress intensity factors. Based on analyses by Potyondy et al. [16, 17] the crack tip stresses are dominated by the membrane K_I and plate k_2 stress intensity factor fields. The membrane K_{II} is very small since the crack turns in the direction to minimize this, and the bending k_1 is small due to the position of the crack in relation to the lap joint. The stiffening provided by the lap joint and stringer suppresses the bending needed to produce a significant k_1 .

3 NUMERICAL PROCEDURES

Solutions for the Kirchhoff theory stress intensity factors exist only for idealized problems such as a crack in an infinite plate. Thus, for both laboratory test specimens and for structural applications, numerical procedures for computing both the Kirchhoff theory and the plane stress theory stress intensity factors are needed. The procedure is to compute components of the crack tip energy release rate from finite element analyses, then calculate K_I , K_{II} , k_1 , and k_2 from the relations between stress intensity factors and these components of the energy release rate.

The finite element computations are performed using the STAGS code [18]. No special crack tip elements are used. Instead, the STAGS 410 element [19], a four-noded, six degree of freedom per node flat plate element, is used. Let us identify the indices $i = 1, 2, 3$ with the nodal displacements in the x_1, x_2, x_3 directions, and the indices $i = 4, 5, 6$ with the nodal rotations about the x_1, x_2, x_3 axes respectively.

The components of energy release rate are given by

$$G_i = \frac{1}{2h\Delta a} F_i \Delta u_i, \quad (2)$$

where h is the plate thickness, Δa is the crack advance (real or virtual), u_1, u_2, u_3 are displacements, u_4, u_5, u_6 are rotations, F_1, F_2, F_3 are forces, and F_4, F_5, F_6 are moments. The Δu_i are the displacement or rotation jumps at a node due to crack advance. In the nodal release method [20] the forces are those at the crack tip node. The Δu_i are the displacement jumps at the former crack tip node that result when the crack is advanced to the next set of nodes, Δa away from the original set. In the modified crack closure method [21] the forces are the nodal forces at the crack tip node, and the displacements are the nodal displacement jumps across the crack at a distance Δa behind the crack tip. The above components of energy release rate are related to the stress intensity factors by [5]

$$\begin{aligned} \frac{K_I^2}{E} &= G_2 + G_6 \\ \frac{K_{II}^2}{E} &= G_1 \\ \frac{\pi}{3E} \left(\frac{1+\nu}{3+\nu} \right) k_1^2 &= G_4 \\ \frac{\pi}{3E} \left(\frac{1+\nu}{3+\nu} \right) k_2^2 &= G_3 + G_5 \end{aligned} \quad (3)$$

In test problems computing the stress intensity factors for the problem of a finite crack in an infinite plate, using a crack tip element size of $a/64$, where a is the crack length, accuracy of approximately 1-3% were obtained, depending on the fracture mode. Recent boundary element analyses have improved this to better than 0.1% for the bending problems [22].

4 EXPERIMENTS

The goal of the experiments was to study fatigue crack growth in sheets under loads that simulate the conditions at the tip of a crack near a lap joint. As discussed above, analyses of this problem show that the loading is primarily membrane Mode-I, (K_I) and bending Mode-2, (k_2). Thus an experiment using a double-edge notched sheet in tension and torsion was developed.

4.1 Test Specimen and Loading

The double edge notched test specimen used is shown in Figure 2. It is cut from sheets of the same 0.090 *in.* thick 2024-T3 aluminum alloy used by Hudson [23]. A summary of the material properties of the alloy is given in Table 1. On each side of the specimen a 0.20 *in.* long, 0.008 *in.* wide starter notch was cut using

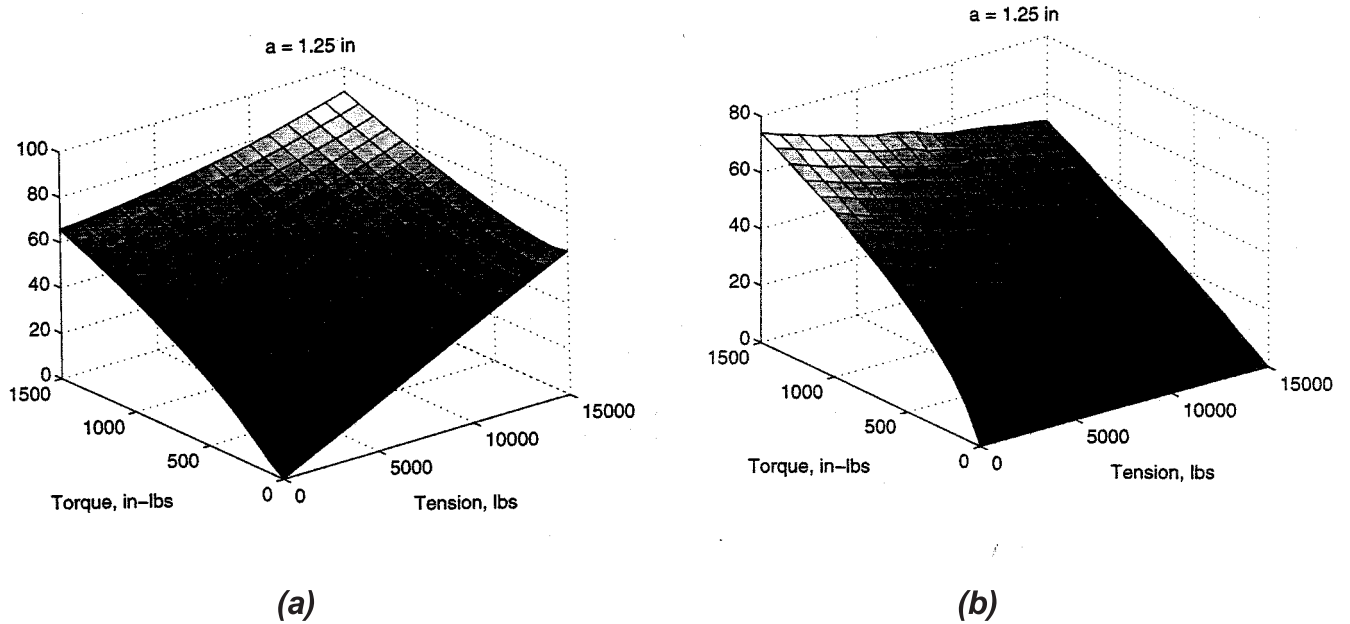


Figure 3: (a) The K_I calibration for the test specimen, at a crack length $a=1.25$ inches. The vertical axis is K_I in units of $\text{ksi}\sqrt{\text{in}}$. (b) The k_2 calibration for $a=1.25$ inches.

electric discharge machining. The crack is in the L-T orientation. To make the fatigue crack more visible, the samples were polished to a $3\mu\text{m}$ finish.

The specimens are gripped by mounting between a steel block and face plate. The block and face plate have slots machined in them that accept a steel rod. When the specimen is clamped in place the steel rod indents the sample, ensuring a no slip condition between the sample and grip. The holes in the test specimen are overdrilled so that the clamping bolts never come directly in contact with the specimen.

All of the tests were performed in a digitally controlled, axial-torsional servo-hydraulic testing machine operating in axial force and torque control. In some experiments a cascade mode of control was used whereby the inner control loop was rotation, while the outer loop was torque. This overcomes problems encountered in torsional control due to the highly nonlinear torsional stiffness of a wide plate specimen. Typical tests ran at frequencies of 0.5 to 1.0 Hz. This low speed is due to the relatively large rotations that were needed to achieve the desired torque loadings.

4.2 Numerical Calibration of Test Specimen

For short cracks a reasonably accurate analytical estimate of K_I as a function of the axial load, P , and the torque, T can be obtained based on the stress in a membrane that is twisted and stretched [24]. However, due to the combination of axial and torsional loading and the resulting nonlinear relationships between applied loads and deformation, it was not possible to work out a complete analytical calibration, i.e. $K_I(P, T)$ and $k_2(P, T)$, of the test specimen. Thus the relation between the applied load, torque, crack length and the stress intensity factors, K_I , and k_2 was determined numerically using finite element analyses and the procedures discussed in section 3. The test specimen was modeled as a half-plate with appropriate symmetry and anti-symmetry boundary conditions on the centerline, as shown in Figure 2b. The top of the plate is clamped, and the bottom is attached to a rigid strip to which the tensile and torsional loads are applied. This rigid strip simulates the loading of the specimen via the steel block grips.

The finite element calculations of K_I , and k_2 were carried out over a 10×10 grid of axial force, P , and

torque values, T , ranging from $0 \leq P \leq 15,000 \text{ lbs}$, $0 \leq T \leq 1500 \text{ in-lbs}$, and for five crack lengths, $a = .25, .50, .75, 1.00, 1.25 \text{ in}$. A sample of the results is shown in Figure 3, which plots K_I , and k_2 as functions of (P, T) for $a = 1.25 \text{ in}$. Along the $T = 0$ axis $k_2 = 0$, K_I is linear with P and agrees with the analytical solution for this problem [25]. When $P = 0$, K_I increases with increasing T due to the stretching of the material at the edges as the plate is rotated. For any given value of torque, k_2 decreases when P is increased. This is due to the axial load flattening out the plate. In essence the plate becomes more like a stretched membrane than a plate in bending. For large torques, K_I becomes relatively insensitive to P . Note that the FEM calculations show that K_{II} and k_1 are essentially zero for this test specimen.

4.3 Methods

Although the tension-torsion fatigue test is far from standard, wherever possible, the tests and data reduction were carried out in accordance with the ASTM Standard Test Method for Measurement of Fatigue Crack Growth Rates (E647). To create a sharp, straight starter crack a 0.050 in fatigue precrack was grown from the EDM cut notches by cycling the plate in pure tension at 6Hz with $\Delta K_I \approx 6.0 \text{ ksi}\sqrt{\text{in}}$, $R = 0.7$, where $R \equiv P_{min}/P_{max}$. During the experiments crack lengths were measured approximately every 0.020 in of crack growth using two traveling microscopes, one for each crack. The accuracy of the crack length measurements is estimated to be 0.002 in .

Given the applied axial load and torque, and the measured crack length history, the histories of the stress intensity factors K_I , and k_2 were calculated for each test via a three dimensional interpolation of the FEM calibrations. Data for crack lengths greater than $a = 1.5 \text{ in}$ were discarded since one cannot reliably extrapolate the calibration beyond one crack length increment more than the data set. The lengths of the left and right crack were often unequal. Since the calibrations were performed for equal crack lengths, data for tests with crack lengths that differed by more than approximately 20% were discarded. Crack lengths are based on the length projected onto the original crack path direction. Although, as will be discussed, the cracks tend to grow at a 45° slant to the plate, the stress intensity factors are based on straight through cracks. In this sense, the stress intensity factors are nominal values. The details of the crack slant, and of contact of the crack surfaces will determine the actual crack tip stress intensity factors.

4.4 Experiments Performed

Three sets of fatigue crack growth experiments were performed using the setup described above. The first set are constant load amplitude tests using R ratios of 0.1 and 0.7. The ratios of k_2 to K_I range from 0 to 1, the higher range being comparable to the ratio expected for a crack that lies along a lap joint in a pressurized fuselage. This experiment gives da/dN in the presence of extensive crack face contact. In the second set of experiments crack face contact was artificially eliminated by performing a series of tests with machine cut cracks of increasing crack lengths. The crack growth rate da/dN in the absence of contact, for a single (K_I, k_2) pair is found from this experiment. The third experiment is a set of constant stress intensity factor tests. The reduction in da/dN with increasing crack length and hence contact is quantified by this experiment.

5 EXPERIMENTAL RESULTS

Although the crack tip stresses are a function of both K_I and k_2 , the results are at first presented as fatigue crack growth rate, da/dN versus K_I , the mode-I stress intensity factor alone. Correlating growth rate with an aggregate stress intensity factor that accounts for the energy of both K_I and of k_2 will be explored in section 6.

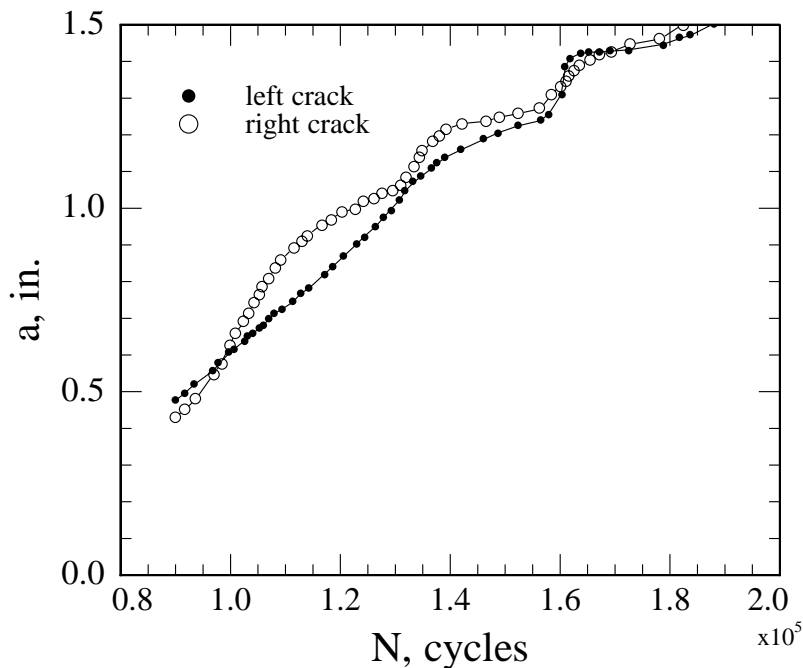


Figure 4: Crack length record for a typical test, number 28, $P = 7000 - 10,000 \text{ lbs.}$ $T = 560 - 800 \text{ in} - \text{lbs.}$ Crack length, a , includes the EDM notch.

5.1 Constant Amplitude Experiments

A total of 36 fatigue crack growth rate tests were performed, 26 at $R = 0.7$, and 8 at $R = 0.1$. Based on the test specimen calibrations the loads were chosen to span $0 < K_I, k_2 < 60 \text{ ksi}\sqrt{\text{in.}}$. The crack length record for a single test is given in Figure 4. The crack growth rate data, Figures 5,6 are plotted in the usual manner, da/dN versus ΔK_I on a log-log scale. In addition to the experimental data two additional lines are plotted to serve as benchmarks for the pure ΔK_I rate for this material. The two lines are based on the crack growth rate correlation

$$da/dN = C(\Delta K_I)^m . \quad (4)$$

The solid lines marked "Hudson" use C and m values from [23] for $R = 0.7$. The dashed lines use values based on our own experiments on the same material. The slight differences in these pure mode-I results are likely due to differences in testing conditions, such as humidity.

The results from a single test run at $P = 7000$ to 10000 lbs. and $T = 560$ to $800 \text{ in} - \text{lbs.}$ are shown in Figures 4 and 5. The loading corresponds to $\Delta K_I = 8.8$ and $\Delta k_2 = 1.6 \text{ ksi}\sqrt{\text{in.}}$ at the start of the test ($a = .4 \text{ in.}$) and $\Delta K_I = 17.2$, $\Delta k_2 = 14.2 \text{ ksi}\sqrt{\text{in.}}$ at the end of the test ($a = 1.5 \text{ in.}$). Thus as the test progresses, the ratio $\Delta k_2/\Delta K_I$ increases from .18 to .8. The results from this test are typical. As seen in Figure 4, the crack grows in steps. The initial rate of growth is fast, then it slows down, almost to a stop, followed by a short period of rapid growth, then slows down again. This pattern is repeated several times. The resulting crack growth rate, shown in Figure 5, shows that initially the crack grows faster than pure Mode-I loading, but as the crack grows the growth rate not only does not increase (despite the increasing stress intensity factors), but drops significantly, followed by extreme fluctuations associated with the crack

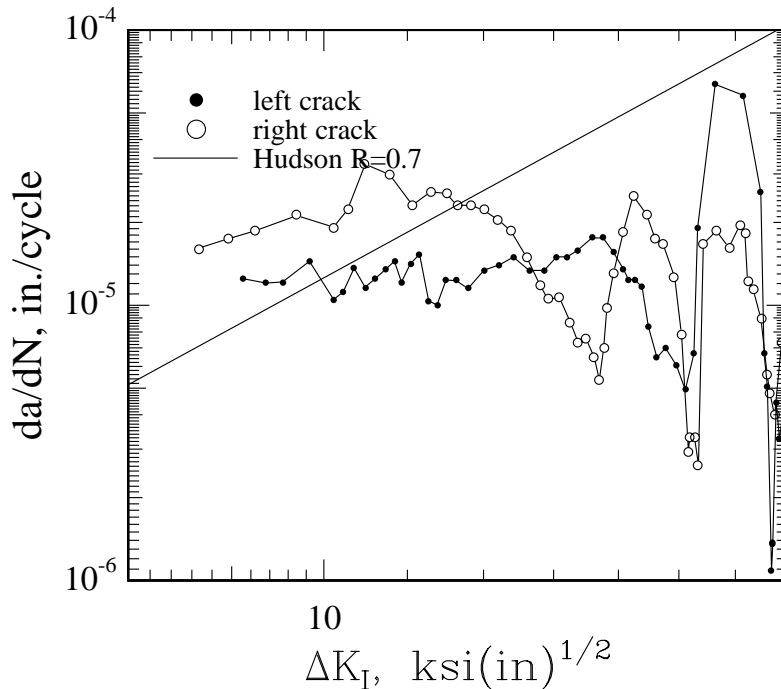


Figure 5: Crack growth rate, da/dN versus ΔK_I for test 28. The solid line is the pure Mode-I benchmark data of Hudson [23].

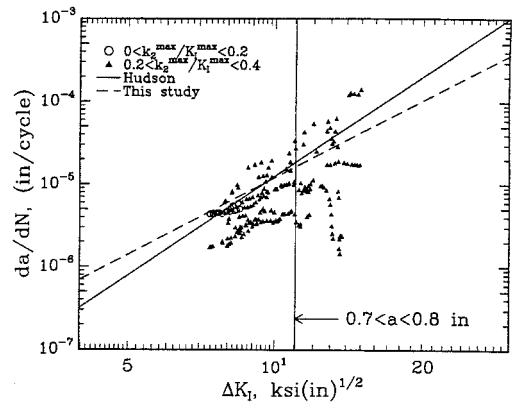
stop-start episodes.

Figure 6 shows similar data. Here data from all of the tests are given in three plots separated by the range of the ratio $\Delta k_2/\Delta K_I$. In Figure 6a, where $\Delta k_2/\Delta K_I < 0.4$ the crack growth rate generally starts out close to the pure Mode-I benchmark, but then drops and fluctuates as the crack extends past a distance of approximately 0.7 in. In Figure 6b, where $0.4 < \Delta k_2/\Delta K_I < 0.7$ the initial rate of growth is somewhat higher than the pure Mode-I case. Again, as the crack extends past approximately 0.7 in. the rate drops and fluctuates. Figure 6c shows the results for $0.7 < \Delta k_2/\Delta K_I < 1.0$ Here da/dN is initially much higher than the pure Mode-I case, but drops dramatically as the cracks grow.

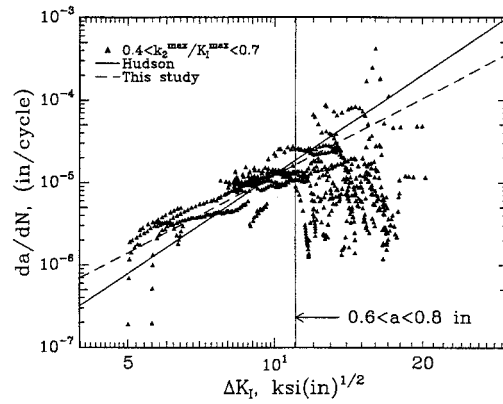
The general observation is that the rate of crack growth drops as the crack grows. This was observed to be associated with the crack faces contacting each other during the fatigue tests. A black oxide powder could be seen falling from the crack tip in many of the tests. A grinding noise due to the crack surfaces coming into contact could be heard. The fracture surfaces were observed to be blackened. Examination in a scanning electron microscope revealed regions of abrasion and wear on the crack faces.

5.2 Crack Growth in Absence of Crack Face Contact

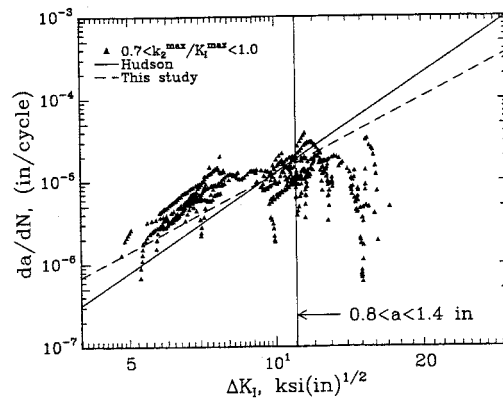
The constant amplitude experiments demonstrate that contact of the crack faces greatly reduces crack growth rate. This is not a totally new phenomenon, although its dominance was unexpected in this problem. Similar observations have been reported in Mode-III fatigue of cylinders loaded in cyclic torsion [26, 27, 28, 29, 30]. The main conclusion from these studies relevant to the current study is that nominal ΔK_{III} does not correlate torsional fatigue crack growth rate data.



(a)



(b)



(c)

Figure 6: Mixed-mode fatigue crack growth rate results. The solid and dashed lines represent the crack growth rate for pure Mode-I loading. The vertical line indicates the range of crack lengths present in this data when $\Delta K_I = 11 \text{ ksi}\sqrt{\text{in}}$. $R = 0.7$. (a) Relatively low values of k_2 . (b) The medium range of values of k_2 (c) Relatively large values of k_2

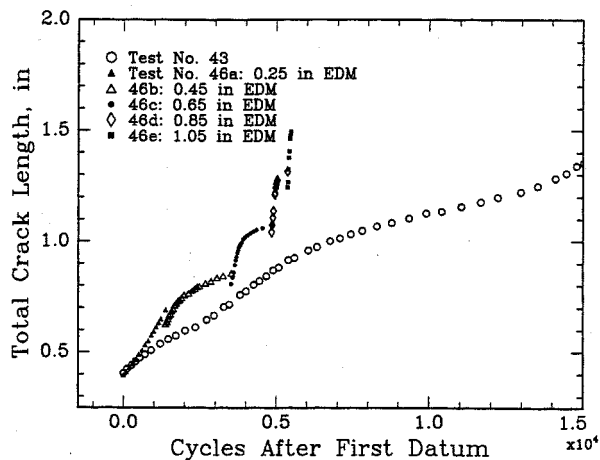


Figure 7: Total crack length versus elapsed cycles from tests in which the crack wakes were removed by using longer machined notches. $R = 0.1$.

In order to begin to quantify the reduction in growth rate due to contact we need to know the intrinsic growth rate, i.e. the growth rate under mixed mode loading in the absence of contact. This was found by performing a series of six tests, all at the same load and torque but with different length EDM starter notches. All of the notched samples were precracked at $\Delta K_I \approx 6 \text{ ksi}\sqrt{\text{in}}$. All tests were carried out at the same loads. An R ratio of $R = 0.1$ was used for these tests. The crack lengths versus cycles are shown in Figure 7. In the first test, number 43, the crack was allowed to grow to a length of 1.4 in. In the next five tests, numbers 46a-e, the crack was started at different initial lengths and allowed to grow for small distances. The first plotted point for tests 46a-e are artificially shifted to the right by adding the summed total cycle count from the previous tests to the cycles of the first point (which would be zero if tests 46a-e were plotted individually.)

The results in Figure 7 are striking in that the removal of the initial roughness-induced closure leads to "pure" mixed-mode crack growth rates much faster than if closure is allowed to evolve as in test 43. The development of contact in the crack wake is particularly well reflected in the curves for 46b and c, where the growth rate starts out fast then steadily decreases.

The da/dN versus ΔK_I results from these tests are shown in Figure 8, along with the Hudson benchmark for $R = 0$. As expected based on the results for $R = 0.7$ tests, the growth rate for test 43 decreases steadily as the crack grows, due to increasing length of contact behind the crack. The initial growth rates for tests 46a-e are connected with a dashed line in the figure. It is seen that the initial growth rates are well above the pure mode-I benchmark data of Hudson. In each case, however, as the crack grows and a region of contact behind the crack develops the growth rates drop to well below the pure mode-I rates.

5.3 Constant Δk_2 Tests

Two important observations from the previous sections are that under mixed mode K_I and k_2 loading of thin plate, there is significant reduction in crack growth rate da/dN with crack growth (Δa), and the crack growth rate in the absence of crack face contact can be higher than benchmark Mode-I rates.

In the experiments described in the previous sections, the stress intensity factors increase as the crack grows. To isolate the effects of increasing crack length and hence of increasing region of crack face contact, a

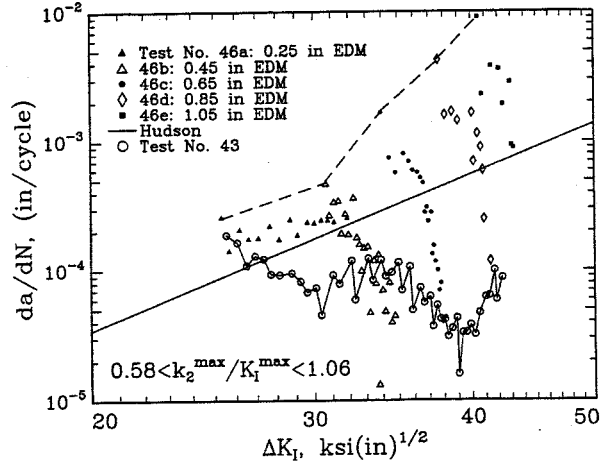
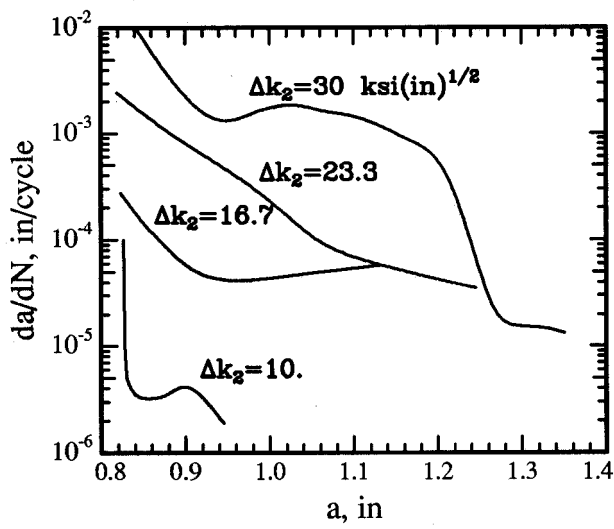


Figure 8: Mixed-mode fatigue crack growth rate in the absence of crack contact (dashed line) and with contact (solid line connecting points.) $R = 0.1$.

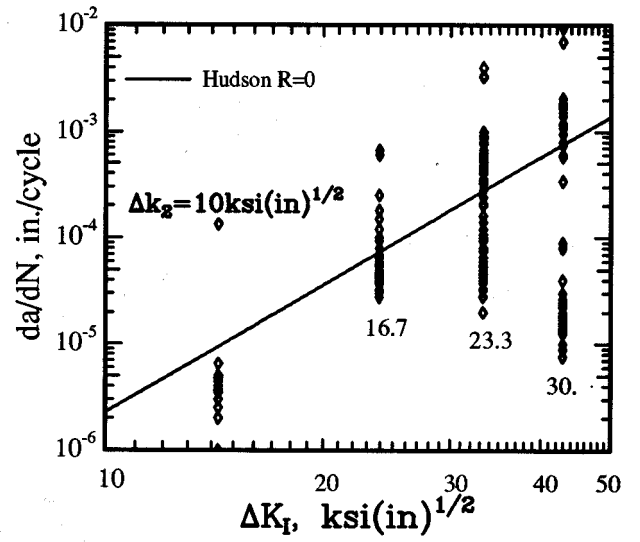
series of tests were performed holding Δk_2 and ΔK_I constant. The tests were all performed with $\Delta k_2 / \Delta K_I = 0.7$, and $R = 0.1$. With these parameters fixed, once a value of Δk_2 was chosen the other stress intensity factors, $K_{I_{max}}$, $K_{I_{min}}$, $k_{2_{max}}$, $k_{2_{min}}$ are fixed (hence the name constant Δk_2 tests). Using the test specimen calibration, the required axial load and torque at a given crack length - for given values of K_I and k_2 are interpolated. As the crack grows the loads are decreased to maintain constant Δk_2 . This was performed in a stepwise manner. That is, at crack growth increments of approximately 0.050 in, the test was paused and crack length readings were made. The loads were then adjusted downwards to get back to the desired constant values of the stress intensity factors. Thus, by adjusting the loads, we try to maintain all K values constant even as crack continues to grow. This is not perfect method; between readings the cracks grow and the K values increase. However, since the loads were adjusted at small increments of crack growth, ΔK_I was held constant to within 2.5% and Δk_2 to within 5%. Tests were performed for four values of Δk_2 , 10, 16.7, 23.3 and 30 $ksi\sqrt{in}$. The highest value of Δk_2 was limited by the testing machine capacity. At each value of Δk_2 , three tests were performed.

The crack lengths are reported as the average of the right and left edge cracks. For at least two of the three tests at each of the Δk_2 values, the right and left crack lengths remained within 5% of each other and for the remaining samples, these remained within 10%. It was observed that if the fatigue precracks on both sides were within 0.002 in, then both cracks grew almost identically.

The results of these experiments are summarized in Figure 9. Figure 9a presents the growth rate versus crack length for all four values of Δk_2 . All of the experiments started with the same crack length, $a = 0.8$ in. The lines plotted in the figure are spline fits to the actual data. The curves all have some common features. The rate of growth initially drops rapidly, then more slowly, coming to an approximately steady value. Both the initial and average crack growth rates increase with increasing stress intensity factors. The final growth rates for $\Delta k_2 = 16.7$, 23.3, and 30 $ksi\sqrt{in}$ are all approximately the same, around $5 - 9 \times 10^{-4}$ in/cycle. The growth rates are plotted vs. ΔK_I in Figure 9b, along with the benchmark data for pure Mode-I loading. The results are similar to those of Figure 8. The addition of the k_2 loading increases the initial rates of crack growth to be significantly higher than the pure Mode-I results. As the cracks grow, the rates drop below the pure Mode-I line. For the three highest Δk_2 values, the cracks must grow by 0.1 to 0.4 in. before da/dN drops below the Mode-I line. We can identify the initial rates of growth as the intrinsic growth rates, i.e.



(a)



(b)

Figure 9: Constant Δk_2 tests. (a) Crack growth rate versus crack length for $\Delta k_2/\Delta K_I = 0.7.$, $R = 0.1$. The lines represent spline fits to the data. One to three tests were run at each value of Δk_2 . (b) da/dN vs. ΔK_I . Increasing crack lengths correspond to decreasing growth rate in this plot.

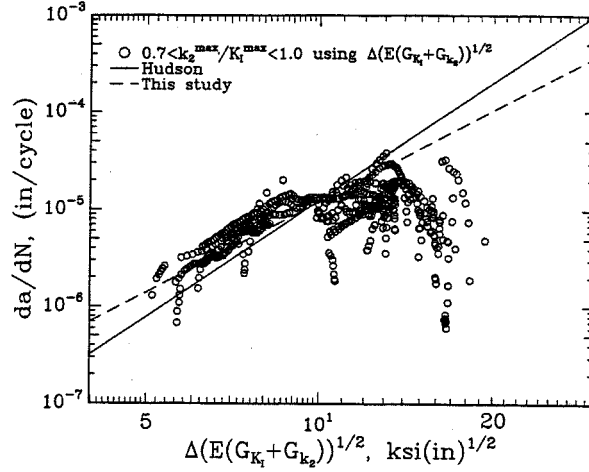


Figure 10: Fatigue crack growth rates from Figure 6c plotted using $\Delta\sqrt{E(G_{K_I} + G_{k_2})}$.

da/dN in the absence of contact. Thus the constant Δk_2 experiments confirm that in the absence of contact, the addition of k_2 loading increases the crack growth rate compared to that for pure K_I loading. However, as in the previous sections, the presence of Δk_2 leads to large scale crack face contact, leading eventually to reducing da/dN to below that for pure Mode-I.

6 DISCUSSION

6.1 Crack Growth in the Absence of Crack Face Contact

The results given in Figures 6 and 9 show that in the early stages of crack growth, when there is a minimal crack wake, and hence minimal crack face contact, for a given ΔK_I , the crack grows faster in the presence of Δk_2 loading than without Δk_2 loading. The data are insufficient to try to construct a sophisticated correlation equation for da/dN as a function of ΔK_I and Δk_2 . However a relatively simple correlation can be attempted that brings the data into rough agreement with Hudson's pure Mode-I results. In Figure 10, the data from Figure 6c, the set of $R = 0.7$ data for which $\Delta k_2 > 0.7\Delta K_I$, are presented using the correlation suggested by Lemaitre et al. [31], where ΔK_I in eq. (4) is replaced by an aggregate value,

$$\begin{aligned} \Delta K_I^{aggregate} &= \Delta\sqrt{E(G_{K_I} + G_{k_2})} \\ \sqrt{E(G_{K_I} + G_{k_2})} &= \sqrt{K_I^2 + \frac{\pi}{3}\left(\frac{1+\nu}{3+\nu}\right)k_2^2}, \end{aligned} \quad (5)$$

with $\nu = .3$. The aggregate ΔK_I simply adds in the energy release rate due to k_2 . This has the effect of moving all of the data points to the right. The result is that the initial rates of growth are now much better correlated with the pure Mode-I rates (compare Fig. 6c to 10), but are still somewhat higher than the pure Mode-I rates. One could experiment with different ways to replace ΔK_I in eq. (4) to see what would correlate best with the pure Mode-I data. It would appear that the aggregate ΔK_I should weigh the energy from k_2 somewhat more heavily than that from K_I in order to move the data points in Figure 6c further to the right. However, any attempt to do so with the present data would not be justifiable, due to the presence of crack face contact.

The same correlation can be attempted with the $R = 0.1$ data in Figure 9b. Here the ratio of the modes is fixed at $\Delta k_2 = 0.7\Delta K_I$. Using $R = 0.1$ it turns out that $\Delta K_I^{aggregate} \approx 1.1\Delta K_I$. This will shift the points in Figure 9b to the right, but not by enough to have them fall on the pure Mode-I line.

Thus for both $R = 0.7$ and $R = 0.1$ the presence of k_2 loading increases da/dN . The effect appears to be stronger for $R = 0.1$ than for $R = 0.7$. Correlating da/dN in the absence of contact with the aggregate ΔK_I given in eq. (5) moves the mixed mode data closer to the pure Mode-I curve but it is still high.

6.2 Crack Orientation

During the pre-cracking, when the sample is loaded in pure Mode-I at $\Delta K_I = 5ksi\sqrt{in}$ the crack grows on a plane perpendicular to the plate surface. Upon application of the mean torsion, just prior to starting the fatigue test the crack transitions to a 45° slant fracture as shown in Figure 11c. The orientation was generally in the direction shown in the figure, i.e. the orientation that will cause the crack surfaces to contact to the greatest degree. It is at first surprising that the crack takes this orientation, rather than the opposite direction which would minimize contact and hence let the crack run most freely. However a detailed look at the crack tip stress distribution shows why this orientation occurs.

For pure k_2 loading the out-of-plane displacement field, w , is given by

$$w = k_2 \frac{(2r)^{3/2}(1-\nu^2)}{2Eh(3+\nu)} \left[\frac{1}{3} \left(\frac{5+3\nu}{1-\nu} \right) \sin\left(\frac{3\theta}{2}\right) - \sin\left(\frac{\theta}{2}\right) \right]. \quad (6)$$

Let $k_2 > 0$. Then on the upper crack face, $\theta = +\pi$, $w < 0$. On the lower crack face, $\theta = -\pi$, $w > 0$. From equation (1), just ahead of the crack, on $\theta = 0$, the shear stress σ_{12} is positive on the front surface, $x_3 = +h/2$, and negative on the back surface, $x_3 = -h/2$. A sketch of the situation is shown in Figure 11a. The positive shear stress on the front surface will tend to drive the cracks down at an angle perpendicular to the direction of maximum principle stress. The negative shear stress on the back surface will tend to drive the cracks upwards at an angle. The result is that the crack tends towards the orientation shown in Figure 11b. That is, due to the crack tip in-plane shear stresses on the surface of the plate, the cracks evolve to a 45 deg slant oriented in the direction that maximizes crack surface contact. In the center of the plate the in-plane shear stresses are zero, but the out of plane shear stresses are not. From equation (1), on $\theta = 0$, $\sigma_{23} < 0$. As sketched in Figure 11c, this would tend to drive the crack in the orientation opposite of the one driven by the surface in-plane shear stresses. Based on the experimental observations it can be concluded that the driving force of the surface in-plane stresses dominates over the center out-of-plane stress in determining the crack orientation behavior.

6.3 Crack Face Contact

The three experiments all show that as the cracks grow the growth rate drops dramatically after some time. This happens when the stress intensity factors are increasing, such as in the constant load amplitude tests, and when the stress intensity factors are held constant as in the constant Δk_2 tests. As discussed above the cracks orient themselves such that the crack surfaces are forced to come into contact as they try to slide past each other in response to the k_2 loading at the crack tip.

This result can be understood in the context of a crack tip shielding model. Due to the nature of the contact any modeling effort will most likely be based on a phenomenological approach. For the time being, if we believe in evolving some law similar to Paris' for the situation at hand, we should note that the simplicity and hence the strength of Paris law comes from the fact that crack growth rate da/dN is a monotonically increasing function of stress intensity factor. However, it is found that da/dN at times decreases with increasing stress intensity factors. This apparent paradox can be resolved if we recognize that crack growth is governed not by the stress intensity factors computed ignoring contact, but by the stress intensity factors at the crack tip. Due to crack face contact, friction and associated load transfer the stresses at the crack tip are reduced substantially.

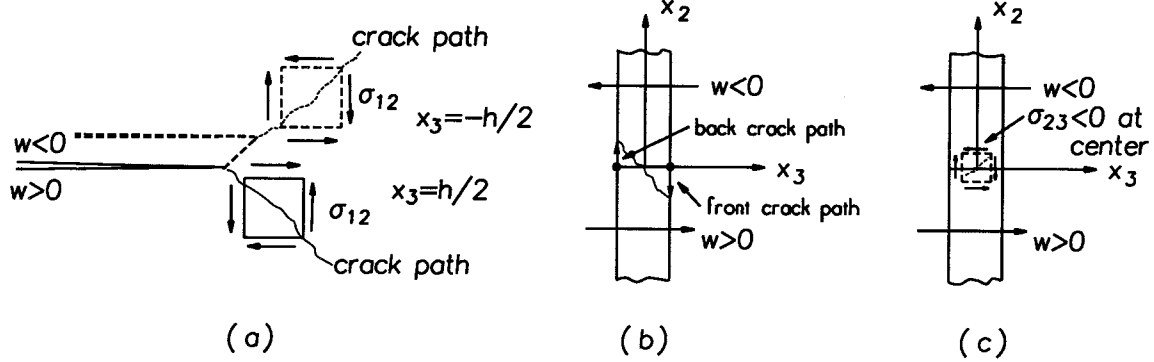


Figure 11: Stress distributions and displacements for $k_2 > 0$. (a) Looking onto the plate surface. (b) Looking from behind the crack (c) Orientation of the shear stress σ_{23} in the plate center, ahead of the crack.

A simple shielding model is that the stresses at the crack tip are governed by the actual stress intensity factors,

$$\begin{aligned} K_I^{actual} &= K_I - K_I^{contact} \\ k_2^{actual} &= k_2 - k_2^{contact} . \end{aligned} \quad (7)$$

The first terms on the right hand sides of the above are the stress intensity factors computed ignoring contact (which is what we have done in the FEM calibrations). The second terms represent the stress intensity factors due to contact. As the crack faces come into contact, stresses are transferred from the crack tip to the crack faces, thus reducing the crack tip stress intensity factors.

Such an approach was used successfully by Gross [32] in his theoretical study of the effect of friction on the growth rate of circumferential cracks in cylinders under cyclic torsion. Gross presented a simple, but robust model that estimates the shielding due to crack face friction, and helps to explain and correlate the data from Tschegg's experiments. In this model, the fracture surface asperities are assumed to act collectively as an edge dislocation producing a fixed displacement of the crack surfaces. Based on this displacement, the crack surface normal stresses are computed. The crack surface friction stresses are then computed based on Coulomb friction. These stresses, when integrated in the appropriate manner give a value for $K_{III}^{contact}$. This value, when subtracted from K_{III} computed neglecting friction, appears to correlate the crack growth data well.

Significant advances have been made recently in both computational techniques for nonlinear problems and in frictional modeling [33]. To actually compute the stress intensity factors due to contact is beyond the scope of the present work. However, based on Gross's work and on the tools now available, we believe that the development of a semi-analytical/numerical model to predict the effect of crack face contact in plates is possible. Our hypothesis is that when such a model is developed, we will be able to correlate da/dN under K_I , k_2 loading with a Paris like equation, and hence provide a method for accurate prediction of fatigue crack growth rate in plates and shells under mixed-mode tension and out-of-plane shear loading.

7 SUMMARY AND CONCLUSIONS

Motivated by the problem of mixed mode fatigue fracture in cracked, pressurized aircraft fuselages, theoretical, numerical and experimental work was performed to provide a more fundamental understanding of the mechanics of this situation. Geometrically nonlinear finite element analyses have been described and tested to ensure accuracy of the resulting stress intensity factor calibrations. The techniques of virtual crack extension, nodal release and modified crack closure have all been tested and shown to be accurate for determining stress intensity factors.

The experimental procedures and results are discussed in detail. The results show, perhaps for the first time, evidence for the dominant influence of crack closure on thin plate mixed-mode fracture. In the absence of crack face contact, and the resulting friction, the addition of the out-of-plane shear loading increases the fatigue crack growth rate. However, as the crack grows, contact inevitably occurs, resulting in a greatly reduced, and somewhat chaotic rate of crack growth. Attempts to correlate growth rate with an aggregate stress intensity factor succeed up to the point where contact becomes important.

Further progress in this problem requires the explicit modeling of the crack face contact/friction problem so that the shielding of the crack tip can be computed. Such an analysis and model must, to be usable, be placed in a framework of engineering computations, i.e. not be so complex that it cannot be applied, but complete enough to adequately represent the physics of the problem. Based on the success of models of fatigue in cylinders under cyclic torsion we believe that a model for plates can be developed.

ACKNOWLEDGEMENTS

This work was supported by NASA Langley's Aircraft Structural Integrity Program, NAG-1-1311. The authors are grateful to Drs. Charles Harris and James Newman of NASA for their support and advice. The experiments were performed using a testing machine upgraded to digital control with support from the NSF through grant CMS-9411791. The computations were performed using IBM RS/6000 computers purchased through an AFOSR grant, F49620-93-1-0235. Use of the Central Computing Facility of the Cornell Center for Materials Research, funded by the NSF through grant DMR 962275 is also acknowledged. The authors are also grateful to Drs. Charles Rankin and Harold Cabiness of Lockheed-Martin for support on the use of the STAGS code, and to Profs. Hui, Ingraffea and Conway of Cornell for their many discussions with us related to this work.

References

- [1] M.J. Viz (1996) *Fatigue Fracture of 2024-T3 Aluminum Plates Under In-Plane Symmetric and Out-of-Plane Antisymmetric Mixed-Mode Deformations*, Ph.D. Thesis, Cornell University.
- [2] C.Y. Hui, and A.T. Zehnder (1993) A Theory for the Fracture of Thin Plates Subjected to Bending and Twisting Moments, *International Journal of Fracture*, **61**, 211-229.
- [3] A.T. Zehnder, M.J. Viz, and A.R. Ingraffea, (1992) Fatigue Fracture in Thin Plates Subjected to Tensile and Shearing Loads: Crack Tip Fields, J Integral and Preliminary Experimental Results, *Proceedings of the VII International Congress on Experimental Mechanics*, Society for Experimental Mechanics, Bethel, CT, 44-50.
- [4] A.T. Zehnder, and C.Y. Hui, (1994) Stress Intensity Factors for Plate Bending and Shearing Problems, *Journal of Applied Mechanics*, **61**, 719-722.
- [5] M.J. Viz, D.O. Potyondy, A.T. Zehnder, C.C. Rankin, and E. Riks, (1995) Computation of Membrane and Bending Stress Intensity Factors for Thin, Cracked Plates, *International Journal of Fracture*, **72**, 21-38.

- [6] M.J. Viz, and A.T. Zehnder (1994) Fatigue Crack Growth in 2024-T3 Aluminum Under Tensile and Transverse Shear Stresses, in *FAA/NASA International Symposium on Advanced Structural Integrity Methods for Airframe Durability and Damage Tolerance, NASA CP-3274*, C. Harris, (ed.), 891-910.
- [7] M.J. Viz, A.T. Zehnder, and J.D. Bamford (1995) Fatigue Fracture of Thin Plates Under Tensile and Transverse Shear Stresses, *Fracture Mechanics, 26th Volume, ASTM STP 1256*, Reuter et al. (eds.) American Society for Testing and Materials, Philadelphia, 631-651.
- [8] S. Timoshenko, and S. Woinowsky-Krieger (1959) *Theory of Plates and Shells*, McGraw-Hill, New York.
- [9] M.L. Williams (1961), The Bending Stress Distribution at the Base of a Stationary Crack, *Journal of Applied Mechanics*, **28**, 78-82.
- [10] E. Reissner (1947-48) On Bending of Elastic Plates, *Quarterly of Applied Math*, **5**, 55-68.
- [11] J.K. Knowles, and N.M. Wang (1960) On the Bending of an Elastic Plate Containing a Crack, *Journal of Mathematics and Physics*, **39**, 223-236.
- [12] J.G. Simmonds, and J. Duva (1981), Thickness Effects are Minor in the Energy Release Rate Integral for Bent Plates Containing Elliptic Holes or Cracks, *Journal of Applied Mechanics*, **48**, 320-326.
- [13] C.Y. Hui, A.T. Zehnder, and Y. Potdar (1998) Williams Meets von-Karman: Mode Coupling and Nonlinearity in the Fracture of Thin Plates, *International Journal of Fracture*, **93**, 409-429
- [14] M.L. Williams (1957), On the Stress Distribution at the Base of a Stationary Crack, *Journal of Applied Mechanics*, **24**, 109-114.
- [15] G.C. Sih, P.C. Paris, and F. Erdogan (1962), Crack-tip Stress-Intensity Factors for Plane Extension and Plate Bending Problems, *Journal of Applied Mechanics*, **29**, 306-312.
- [16] D.O. Potyondy (1993) *A Software Framework for Simulating Curvilinear Crack Growth in Pressurized Thin Shells*, Ph.D. Thesis, Cornell University.
- [17] D.O. Potyondy (1994) Discrete Crack Growth Analysis Methodology for Through Cracks in Pressurized Fuselage Structures, in *FAA-NASA International Symposium on Advanced Structural Integrity Methods for Airframe Durability and Damage Tolerance, NASA CP-3274*, C. Harris, (ed.), 581-601.
- [18] Lockheed-Martin Palo Alto Research Laboratory (1996), *Structural Analysis of General Shells*.
- [19] C.C. Rankin, and F.A. Brogan (1991) The Computational Structural Mechanics Testbed Structural Element Processor ES5: STAGS Shell Element, *NASA Technical Report, CR4358*.
- [20] H. Ansell (1988) *Bulging of Cracked Pressurized Aircraft Structures*, Ph.D. Thesis, Linköping University, Sweden. Linköping University Report LIU-TEK-LIC-1988:11.
- [21] E.F. Rybicki, and M.F. Kanninen (1977) A Finite Element Calculation of Stress Intensity Factors by a Modified Crack Closure Integral, *Engineering Fracture Mechanics*, **9**, 931-938.
- [22] A. Frangi (1997) Regularized BE Formulations for the Analysis of Fracture in Thin Plates, *International Journal of Fracture*, **84**, 351-366.
- [23] C.M. Hudson (1969) Effect of Stress Ratio on Fatigue-Crack Growth in 7075-T6 and 2024-T3 Aluminum Alloy Specimens, *NASA TN D5390*.
- [24] H.D. Conway (1998) personal communication.
- [25] H. Tada, P.C. Paris, and G.R. Irwin (1985) *The Stress Analysis of Cracks Handbook, Second Edition*, Paris Productions Inc., St. Louis, Missouri.

- [26] E.K. Tscheegg (1982) A Contribution to Mode III Fatigue Crack Propagation, *Materials Science and Engineering*, **54**, 127-136.
- [27] E.K. Tscheegg (1983) Mode III and Mode I Fatigue Crack Propagation Behaviour Under Torsional Loading, *Journal of Materials Science*, **18**, 1604-1614.
- [28] E.K. Tscheegg, R.O. Ritchie, and F.A. McClintock (1983) On the Influence of Rubbing Fracture Surfaces on Fatigue Crack Propagation in Mode III, *International Journal of Fatigue*, **5**, 29-35.
- [29] E.K. Tscheegg, and S. Suresh (1987) Torsional Fracture of Fatigue Pre-cracked Ceramic Rods, *Journal of Materials Science*, **22**, 2927-2932.
- [30] E.K. Tscheegg, S.E. Stanzl, H.R. Mayer, and M. Czegley (1992) Crack Face Interactions and Near Threshold Fatigue Crack Growth, *Fatigue and Fracture of Engineering Materials and Structures*, **16**, 71-83.
- [31] J. Lemaitre, A. Turbat, and R. Loubet (1977) Fracture Mechanics Analysis of Pressurized Cracked Shallow Shells, *Engineering Fracture Mechanics*, **9**, 443-460.
- [32] T.S. Gross (1985) Frictional Effects in Mode III Fatigue Crack Propagation, *Scripta Metallurgica*, **19**, 1185-1188.
- [33] A. Ruina (1980) Slip Instability and State Variable Friction Laws, *Journal of Geophysical Research*, **88**, 10359-10370.

Elastic Modulus	10,240 ksi
Yield Stress	51.2 ksi
Ultimate Tensile Strength	70.9 ksi
K_{IC}	100. ksi $\sqrt{\text{in}}$

Table 1: Material properties for the L-T orientation of 2024-T3 Aluminum.